HHS Public Access

Author manuscript

Biosens Bioelectron. Author manuscript; available in PMC 2020 February 01.

Published in final edited form as:

Biosens Bioelectron. 2019 February 01; 126: 831–837. doi:10.1016/j.bios.2018.11.052.

A cellulose-based photoacoustic sensor to measure heparin concentration and activity in human blood samples.

Ananthakrishnan Soundaram Jeevarathinam[a], **Navin Pai**[a], **Kevin Huang**[a], **Ali Hariri**[a], **Junxin Wang**[a], **Yuting Bai**[a], **Lu Wang**[a], **Tiffany Hancock**[c], **Stanley Keys**[c], **William Penny**[c], and **Jesse V. Jokerst**[*,a,b]

[a]Department of NanoEngineering, University of California San Diego, La Jolla, California 92093, United States.

[b]Materials Science Program and Department of Radiology, University of California San Diego, La Jolla, California 92093, United States

[c]Cardiology Unit, VA Healthcare System, San Diego, La Jolla, California 92161, United States.

Abstract

Heparin is an indispensable drug in anticoagulation therapy but with a narrow therapeutic window, which dictates regular testing and dose adjustment. However, current monitoring tools have a long turnaround time or are operator intensive. In this work, we describe a cellulose-based photoacoustic sensor for heparin. The sensors have a turnaround time of 6 minutes for whole blood samples and 3 minutes for plasma samples regardless of heparin concentration. These sensors have a limit of detection of 0.28 U/ml heparin in human plasma and 0.29 U/ml in whole blood with a linear response (Pearson's r = 0.99) from 0 – 2 U/ml heparin in plasma and blood samples. The relative standard deviation was <12.5% in plasma and < 17.5% in whole blood. This approach was validated with heparin-spiked whole human blood and had a linear correlation with the activated partial thromboplastin time (aPTT) (r = 0.99). We then studied 16 sets of clinical samples—these had a linear correlation with the activated clotting time (ACT) (Pearson's r = 0.86, P<0.0001). The photoacoustic signal was also validated against the cumulative heparin dose (Pearson's r = 0.80, P<0.0001). This approach could have applications in bed-side heparin assays for continuous heparin monitoring.

Graphical abstract

* jjokerst@ucsd.edu.

Author Contributions

A.S.J. designed the experiments and wrote original draft. N.P. performed aPTT and processing of clinical samples. K.H. and A.H. performed control experiments and imaging of substrates. J.W., Y. B., and L. W contributed to visualization and data presentation. T.H., H. K., and W. P. collected the clinical samples from patients during cardiac procedures. J.V.J. designed experiments, wrote the original draft, and edited the final manuscript.

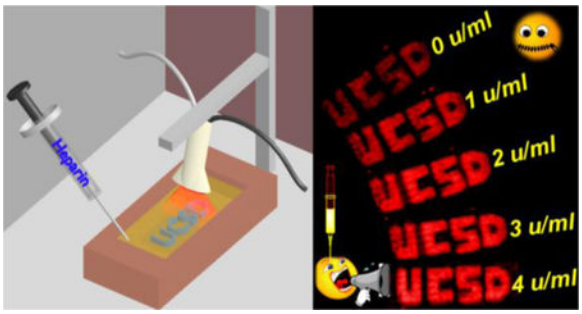

Cellulose-based photoacoustic heparin sensor can monitor therapeutic dose of heparin in whole human blood and plasma samples.

Keywords

Heparin sensing; Photoacoustic imaging; Ultrasound; Anticoagulation therapy; cellulose based sensor

1. Introduction.

Heparin is a popular anticoagulant because it is quick, reversible, and affordable (Farooq et al. 2014), but it also suffers from a narrow therapeutic window and is second most common intensive care unit (ICU) medication error (Wahr et al. 2014). Heparin is a glycosaminoglycan with a negatively charged sulfate group, which complexes with antithrombin to increase the deactivation of thrombin 100–1000-fold. Despite the advent of low molecular weight heparin (LMWH) and direct-acting oral anticoagulants (DOACs) (Antonio et al. 2015), unfractionated heparin is still common because of its quick reversibility (Baluwala et al. 2017).

The activated partial thromboplastin time (aPTT) is the clinical standard for monitoring heparin activity. However, the aPTT suffers from long mean turnaround times (35–280 minutes) (Ojito et al. 2012), poor correlation to outcome, and batch-to-batch variation in reagents (Shetty et al. 2003). Factor Xa analysis reflects the effect of other coagulation factors such as factor IX, factor VIII, and antithrombin, but is generally restricted to research hospitals (Takemoto et al. 2013). The activated clotting time (ACT) and thromboelastography (TEG ®) can be used as point-of-care heparin monitoring tools but require a skilled operator and require special sample preparation. Importantly, these existing techniques are activity-based assays and are susceptible to errors caused by fibrinolysis, platelet dysfunction, hypothermia, hemodilution, and the presence of drugs such as aprotinin (Prisco and Paniccia 2003). Thus, a non-invasive, direct, and rapid point-of-care tool that directly assays heparin and would have value to the community.

Direct detection of heparin under biologically relevant conditions could be useful in monitoring heparin-based therapy. Other approaches utilize micro-electromechanical film bulk acoustic sensors (Chen et al. 2017a; Chen et al. 2017b), nanoparticles (Ma et al. 2014), cationic fluorescent/phosphorescent polymers (Ma et al. 2014; Mehta et al. 2017; Pu and Liu

2009; Shi et al. 2016), and small molecule sensors via aggregation-induced emission (Zheng et al. 2017). Mallard blue dye and gold nanoparticles capable of selectively sensing heparin and other sulfated glycosaminoglycans were also recently described in detail (Bromfield et al. 2013; Kalita et al. 2014; Shriver and Sasisekharan 2013). However, optical strategies are difficult with biological samples due to interferences from proteins, lipids, and ions. Electrochemical techniques for heparin sensing in whole blood samples use voltammetry and potentiometry. However, these systems involve complex instrumentation and interference from albumin in blood samples (Amemiya et al. 2011), which limits sensitivity (Yoshimi et al. 2018).

We recently reported a photoacoustic technique for heparin sensing in whole human blood using methylene blue (Wang et al. 2016). Photoacoustic imaging is a hybrid optical/acoustic technique that uses the pressure waves generated from thermal expansion after optical absorption. It combines the good temporal and spatial resolution of ultrasound with the contrast of optical imaging (Johannes et al.; Pu et al. 2014; Pu et al. 2018; Qin et al. 2017; Stylogiannis et al. 2018; Sun and Emelianov 2018; Wong et al. 2017). We now extend this basic discovery to a more usable sensor based on cellulose. Indeed, paper-based point-of-care diagnostic tools are very attractive because of their rugged nature and low cost (Martinez et al. 2010). The devices are cost effective and easily fabricated into different modalities with microchannels and adjoining zones (Martinez et al. 2010). Paper-based substrates are compatible with a wide variety of analytical techniques. The low cost of paper-based sensors makes it easy to do replicate testing (Chaiyo et al. 2018).

Here, we describe a polyethylene glycol (PEG)-impregnated, Nile blue A-infused, paper-based photoacoustic sensor for directly assaying heparin. This sensor uses fingerprick-sized samples of blood at the point-of-care. The paper-based sensors are physically stable during the analysis and offer a robust platform for bedside heparin assays in whole human blood. Our initial work in photoacoustic-based heparin sensing added methylene blue and heparin to the whole blood of healthy human donors (Wang et al. 2016). This work then described a heparin-sensitive intravenous catheter and tested it with different heparin concentrations in buffer. We now expand this work to include a point-of-care paper-based sensing approach and validated it with 16 human subjects (with ~ 4 different heparin concentrations per patient). These sensors may have utility as a point-of-care technique—especially when combined with low-cost single element transducers and LED excitation sources (Hariri et al. 2018; Zemp et al. 2007).

Materials and Methods

1.1. Photoacoustic characterization of sensors.

The cellulose-based heparin sensors were immobilized on the surface of a glass plate using 3M Millipore tape. A graphite mark served as a reference for any fluctuations in laser power. The 3D images were acquired by moving the transducer across the samples and the graphite reference sample. The photoacoustic intensity was reported either as a raw value or normalized to the graphite signal. Images of the sensors were acquired after each subsequent increase in heparin concentration (sensors were reusable across multiple concentrations of

heparin). All photoacoustic measurements were performed in aqueous conditions (100% humidity) and 20–25 °C.

Photoacoustic study in phosphate buffered saline (PBS).—Glass substrates with the immobilized heparin sensors (0.5 × 0.5 cm) and the graphite reference were immersed inside a petri dish containing 70 ml of 0.01 M PBS (0.137 M NaCl and 0.0027 M KCl). The position of both the petri dish, glass substrate, and sensors were fixed with respect to the transducer. 3D images of the sensors and reference were acquired before addition of heparin and after successive additions of 0.5 U/ml unfractionated heparin (successive 35 μl aliquots of 1000 U/ml heparin). The maximum heparin concentration was 5.0 U/ml. The phosphate buffer medium was thoroughly mixed for 30 s after each addition of heparin, and the sensors were imaged 60 s after addition.

1.2. Photoacoustic study in 50% diluted and undiluted pooled human plasma.

Equal volumes of 0.1 M PBS and normal pooled human plasma were mixed to obtain 50% diluted plasma. Three heparin sensors (0.5 × 0.5 cm) along with the graphite reference were immersed in 50 ml of medium (diluted or undiluted pooled human plasma). 3D images were acquired before and after each incremental addition of 12.5 μl of 1000 U/ml heparin (increase in working concentration of 0.25 U/ml). We mixed the medium thoroughly for 30 s after each heparin increment and then imaged the sensors after waiting for 60 s.

1.3. Photoacoustic characterization of heparin sensors in whole human blood.

Blood was obtained from a healthy donor according to IRB guidelines. The heparin sensors were dipped in 10 ml of whole human blood for 1 minute, rinsed with PBS, and imaged. The blood sample was then spiked with a higher heparin concentration and the procedure repeated. Here, the increase was 0.25 U/ml of heparin (10 μl of 250 U/ml heparin) at each step. The glass slides were imaged under PBS media (50 ml).

1.4. Photoacoustic study of heparin sensing heparin sensors in clinical samples.

We studied 16 sets of clinical samples obtained from 16 patients undergoing invasive clinical cardiac procedures that require anticoagulation with high-dose i.v. heparin. (See Supplementary Information section 1.2 for more details.) All human subject work was done with IRB approval from the UCSD and San Diego Veterans Administration hospital. The heparin sensors and reference were treated with a 30 μl drop of plasma on each of the three sensors using a micropipette. After 4 minutes, the glass slide with the heparin sensors was rinsed twice with PBS and imaged.

2. Results and Discussion

Heparin is a polysulfated glycosaminoglycan (Fig. 1A) with a net negative charge that can interact with cationic dyes such as Nile blue A (Fig. 1B) leading to a spectral change (Fig. 1C and Fig S2; Supplementary Information section 1.5). We created a cellulose-based photoacoustic heparin sensor by loading Nile blue A onto polyethylene glycol (PEG) modified Whatman filter paper substrates (See Supplementary Information Fig. S3 and section 1.6). The sensors showed just 13.4% leaching in PBS media (see Supplementary

Information section 1.6) over a period of 3 h. The PEG and dye content of these sensors were first optimized (Fig. S2). We then evaluated the intra- and inter-assay reproducibility and limit of detection in buffer, plasma, and whole blood. Finally, we compared this method to the aPTT and ACT in whole blood samples from healthy donors and in clinical samples.

2.1. Characterization of cellulose-based heparin sensor in phosphate buffer saline (PBS) and diluted human plasma.

The cellulose-based heparin sensors can respond to heparin via the formation of heparin-Nile blue A aggregates due to electrostatic interaction. The heparin-dye aggregates have a higher photoacoustic activity due to decreased fluorescence, reduced degrees of freedom, and poor heat transfer to the solvent (Wang et al. 2018). This change in photoacoustic signal is directly proportional to the amount of heparin in the medium. First, we studied the photoacoustic response of Nile blue A in aqueous solution (Fig. 1D and Fig. S2). Next, we studied the photoacoustic signal changes in the cellulose-based heparin sensors due to heparin in PBS (Fig. 1E). The LoD in PBS is 1.2 U/ml. There was a surprising small decrease in signal at 0.5 U/mL heparin. When the cellulose sensors were immersed in PBS medium at room temperature for a minimum of minimum of 10 minutes before the study, the decrease was not observed (Fig. S4). The initial decrease is likely due to the initial hydration of the substrate with Nile blue A that is insoluble in PBS medium. The wettability of the paper-based sensors has been shown to have a strong correlation to response time (Tian et al. 2012).

This experiment was repeated with 50% human plasma—raw photoacoustic images are presented in Fig. 1E. The initial decrease in photoacoustic intensity at 0.5 U/ml heparin was not observed (Fig. 1F). The slope in 50% plasma is 53% higher than PBS. The linear correlation of photoacoustic response of sensors was observed between 0 and 2.0 U/ml heparin ($r > 0.97$) in both PBS and diluted plasma. The limit of detection in 50% plasma was 0.02 U/ml, which is well below the therapeutic heparin levels for different clinical procedures such as thromboembolism (7–8 U/ml), acute myocardial infraction (2.5 U/ml), coronary angioplasty (2.0 U/ml), cardiopulmonary bypass (5.6 U/ml), and extracorporeal membrane oxygenation (0.5 U/ml) (Wang et al. 2016). Thus, the utility of this sensor is optimized in the therapeutic range of clinical heparin concentrations. The baseline photoacoustic signal of sensors with the same dimensions differed by 1.5%. The intraassay relative standard deviation in 50% diluted plasma was <6.1%.

2.2. Sensing efficacy in normal pooled human plasma and whole human blood.

Next, we tested the sensor from 0 – 4 U/mL heparin with whole plasma (Fig. 2A). Fig. 2A shows the sensors repeatedly imaged after each addition. The limit of detection in undiluted plasma is 0.28 U/ml with a relative standard deviation <8.2% (Fig. 2B). This trend in photoacoustic response of sensors and signal contrast with low error was also reproducible between independent experiments (Fig. 2C). Thus, the heparin sensors exhibit a high intra- and inter-assay reproducibility in plasma with a maximum inter-assay relative standard deviation of 8.4%.

Finally, we used whole blood (Fig. 3), which can be a challenge due to an increased number of interferences (Bromfield et al. 2013; You et al. 2017). Electrochemical techniques for direct heparin assaying in blood have been demonstrated but suffer from problems in reproducibility and irreversible binding (Amemiya et al. 2011). Fig. 3A contains raw imaging data from 0–2.5 U/mL (note that not all of the raw images are shown; Fig. 3B has more data points). The assay was linear from 0 to 2.0 U/mL (Pearson's r = 0.98) (Fig. 3B). Values above 2.0 U/mL had a plateau effect likely due to saturation of surface-bound Nile blue A dye; fortunately, the linear dynamic range corresponds nicely to the clinically relevant range of 0.5 to 2.0 U/mL.

The limit of detection in whole human blood was 0.28 U/ml. The relative standard deviations in this range were < 17.5% (Fig. 3C). Error sources include background photoacoustic signal from hemoglobin and deoxyhemoglobin due to incomplete rinsing in between different heparin concentrations (note that same sensors were repeatedly imaged after treatment with higher heparin concentration) (Zhang et al. 2007). Finally, we compared the slope of the photoacoustic response in these various sample matrices—the slope (sensitivity) was highest in whole blood followed by plasma and PBS (Fig. 3D). The baseline signal of cellulose sensors was highest for whole blood followed by plasma, 50% diluted plasma, and PBS. We attribute the higher photoacoustic background in blood to the presence of red blood cells. The higher background in plasma and diluted plasma might be due to the affinity of the cationic dyes to plasma constituents (Küçükkılınç and Özer 2007; Strohm et al. 2013). The response was 1.2-fold higher in whole blood samples than plasma; pure plasma was 1.4-fold higher than the response in diluted plasma. The sensitivity in whole blood was ~5-fold higher than in PBS. We attribute this change to interaction of heparin with plasma proteins (Gatti et al. 1979), which increases the affinity of the heparin-protein complex to Nile blue A and stabilizes the heparin/dye complex (Muñoz and Linhardt 2004).

Correlation of photoacoustic response of sensors with aPTT.

Finally, we compared the photoacoustic signal to aPTT values (Fig. 4A). Fig. 4 compares the photoacoustic response to the aPTT of pooled human plasma (Fig. 4A) and plasma from freshly collected whole human blood (Fig. 4B). The aPTT values in commercial pooled human plasma (black data; Fig. 4A) were less linear (Pearson's r = 0.89) as a function of heparin concentration than the response of the photoacoustic sensor to heparin concentration (red data; Fig. 4A) (Pearson's r = 0.99). A plot of photoacoustic response versus aPTT values for the commercial pooled plasma showed a lower linear correlation (r= 0.86) compared to fresh human blood (Pearson's r =0.99) (Fig 4C). This is likely because the whole blood sample was fresh, but the plasma had been previously frozen—freezing can dysregulate clotting factors (Alesci et al. 2009). Regardless, these results suggest that the photoacoustic signal can monitor heparin activity analogously to the aPTT.

2.3. Heparin sensing in banked clinical plasma specimens.

Finally, we analyzed banked (at −80 °C storage) plasma samples collected from 16 patients undergoing ablation in the electrophysiology lab (3 to 10 samples per patient; 78 total samples; Table S1). We plotted the first four samples for each subject because that is the

region where the heparin dose is changing the most rapidly and where anticoagulant activity must be most carefully monitored (n=60 samples). Figure S5A plots the photoacoustic response versus the ACT values with a Pearson's r = 0.76 (P<0.0001).

We binned the photoacoustic response as a function of cumulative heparin dose and ACT (Fig. 5A)—the ACT values measured over all sample sets were compiled into 20-s bins. We then averaged the photoacoustic intensity within each of these bins and plotted against the averaged ACT values (Fig. 5(A)). The average photoacoustic intensity had a linear correlation against average ACT (Pearson's r = 0.86); 62.5% of the measured photoacoustic intensity values were within the 95% CI band (Fig 5(A)). The change in photoacoustic intensity with respect to the ACT values are significant (P < 0.0001). This binning was used to reduce inherent errors associated with the measurements. Variations in ACT include different baseline ACT values, choice of activator, presence of drugs such as aprotinin, and the instrument used (Perry et al. 2010). Error sources associated with photoacoustic data include the variation in the size of the sensors and variation in dye distribution across the sensor area.

Next, we correlated the photoacoustic response to ACT and cumulative heparin dose. This correlation was linear and significant for both ACT and cumulative heparin dose (Fig 5 (A) and (B); P < 0.0001; Pearson's r > 0.7). The aPTT values were all over 500 s and had little utility with these samples (Baglin et al. 2006). However, this study demonstrated a close correlation between the photoacoustic signal of the heparin sensor and the ACT (r = 0.86; P < 0.0001) suggesting that this approach is not only measuring heparin concentration but also acts as a surrogate for anticoagulant activity.

This approach can quickly measure heparin in small samples (~ 50 μL). Other recently reported dye-based heparin assays are more selective but have not yet been studied in complex biological samples (Bromfield et al. 2013; Buee et al. 1991). Colorimetric assays for heparin are either limited to plasma or buffer or have not yet been demonstrated in whole blood (Mehta et al. 2017; Templeton 1988; You et al. 2017). The aPTT is limited by its range of detection, variation in reagents, and instrumentation (Baglin et al. 2006; Lehman and Frank 2009). The Factor-Xa test is a chromogenic assay that measures the activity of heparin against activated factor X. However, the anti-Xa test underestimates heparin content in the presence of antithrombin deficiency, post-thrombolysis, hyperbilirubinemia, end stage renal disease, and pregnancy (Vera-Aguilera et al. 2016). The ACT is currently used in the operating room as a heparin monitor but has some insensitivities to coagulation abnormalities and platelet deficiencies—having a direct heparin assay could offer insight into the patient's anticoagulation status (Maxwell et al. 2011). The detection limit achieved here (0.28 U/ml in whole human blood samples) is consistent with clinically relevant doses (Murray et al. 1997) including those needed for thromboembolism (7–8 U/ml) (Gould et al. 1999), acute myocardial infraction (2.5 U/ml) (Luigi 1989), coronary angioplasty (2 U/ml) (Narins et al. 1996), cardiopulmonary bypass (5.6 U/ml) (Wright et al. 1993), and extracorporeal membrane oxygenation (ECMO) (Baird et al. 2007).

3. Conclusion.

This study described the preparation of a cellulose-based heparin sensor and photoacoustic imaging to measure heparin in blood samples. The correlation with cumulative heparin levels (Fig. 5), turnaround time, and sample requirements are comparable to the ACT. Further, the photoacoustic response of heparin sensors in different sample matrix are closely correlated with aPTT and ACT suggesting that this method is monitoring heparin activity—not just concentration. The paper-based heparin sensors are very affordable and can be used as a disposable sensor. Our next steps will optimize this technique into a bedside and/or point-of-care heparin assay. The limitations of the work originate from the fact that it is a direct heparin assay and the anticoagulant activity is a result of heparin-antithrombin complex. However, this study demonstrated a close correlation to activity-based assay (ACT and aPTT). Future work will translate this technology into an implantable catheter device for real-time *in vivo* monitoring of heparin concentrations.

Supplementary Material

Refer to Web version on PubMed Central for supplementary material.

Acknowledgements

We acknowledge funding from DP2 HL137187 and infrastructure from S10 OD021821.

Appendix A.: Supplementary material

Supplementary data associated with this article can be found in the online version

References

Alesci S, Borggrefe M, Dempfle C-E, 2009 Effect of freezing method and storage at −20 °C and −70 °C on prothrombin time, aPTT and plasma fibrinogen levels. Thrombosis Research 124(1), 121–126. [PubMed: 19128820]

Amemiya S, Kim Y, Ishimatsu R, Kabagambe B, 2011 Electrochemical heparin sensing at liquid/liquid interfaces and polymeric membranes. Anal. Bioanal. Chem 399(2), 571–579. [PubMed: 20686753]

Antonio GO, Luisa SGM, Ramón L, Isabel TFA, Emilio VC, 2015 Direct-acting oral anticoagulants: pharmacology, indications, management, and future perspectives. European Journal of Haematology 95(5), 389–404. [PubMed: 26095540]

Baglin T, Barrowcliffe TW, Cohen A, Greaves M, 2006 Guidelines on the use and monitoring of heparin. Br. J. Haematol 133(1), 19–34. [PubMed: 16512825]

Baird CW, Zurakowski D, Robinson B, Gandhi S, Burdis-Koch L, Tamblyn J, Munoz R, Fortich K, Pigula FA, 2007 Anticoagulation and pediatric extracorporeal membrane oxygenation: impact of activated clotting time and heparin dose on survival. Ann Thorac Surg 83(3), 912–919; discussion 919–920. [PubMed: 17307433]

Baluwala I, Favaloro EJ, Pasalic L, 2017 Therapeutic monitoring of unfractionated heparin - trials and tribulations. Expert Rev. Hematol 10(7), 595–605. [PubMed: 28632418]

Bromfield SM, Barnard A, Posocco P, Fermeglia M, Pricl S, Smith DK, 2013 Mallard Blue: A High-Affinity Selective Heparin Sensor That Operates in Highly Competitive Media. J. Am. Chem. Soc 135(8), 2911–2914. [PubMed: 23406254]

Buee L, Boyle NJ, Zhang L, Delacourte A, Fillit HM, 1991 Optimization of an alcian blue dot-blot assay for the detection of glycosaminoglycans and proteoglycans. Analytical Biochemistry 195(2), 238–242. [PubMed: 1750673]

Chaiyo S, Mehmeti E, Siangproh W, Hoang TL, Nguyen HP, Chailapakul O, Kalcher K, 2018 Non-enzymatic electrochemical detection of glucose with a disposable paper-based sensor using a cobalt phthalocyanine–ionic liquid–graphene composite. Biosensors and Bioelectronics 102, 113–120. [PubMed: 29128713]

Chen D, Song S, Ma J, Zhang Z, Wang P, Liu W, Guo Q, 2017a Micro-electromechanical film bulk acoustic sensor for plasma and whole blood coagulation monitoring. Biosensors and Bioelectronics 91, 465–471. [PubMed: 28068607]

Chen D, Zhang Z, Ma J, Wang W, 2017b ZnO Film Bulk Acoustic Resonator for the Kinetics Study of Human Blood Coagulation. Sensors 17(5).

Farooq MS, Farooq MZ, Khan S, 2014 Should warfarin and heparins be replaced by the new oral anticoagulants? Drug Res. (Stuttgart, Ger.) 64(12), 695–696, 692 pp.

Gatti G, Casu B, Hamer GK, Perlin AS, 1979 Studies on the Conformation of Heparin by 1H and 13C NMR Spectroscopy. Macromolecules 12(5), 1001–1007.

Gould MK, Dembitzer AD, Doyle RL, Hastie TJ, Garber AM, 1999 Low-molecular-weight heparins compared with unfractionated heparin for treatment of acute deep venous thrombosis: A meta-analysis of randomized, controlled trials. Ann. Intern. Med 130(10), 800–809. [PubMed: 10366369]

Hariri A, Lemaster J, Wang J, Jeevarathinam AS, Jokerst JV, Chao DL, Jokerst JV, Jokerst JV, 2018 The characterization of an economic and portable LED-based photoacoustic imaging system to facilitate molecular imaging. Photoacoustics 9, 10–20. [PubMed: 29234601]

Johannes R, Héctor E, Sven G, Gali S, Michael Z, Georg W, Vasilis N, Daniel R, Dual-Wavelength Hybrid Optoacoustic-Ultrasound Biomicroscopy for Functional Imaging of Large-Scale Cerebral Vascular Networks. Journal of Biophotonics 0(ja), e201800057.

Kalita M, Balivada S, Swarup VP, Mencio C, Raman K, Desai UR, Troyer D, Kuberan B, 2014 A Nanosensor for Ultrasensitive Detection of Oversulfated Chondroitin Sulfate Contaminant in Heparin. J. Am. Chem. Soc 136(2), 554–557. [PubMed: 24127748]

Küçükkılınç T, Özer İ, 2007 Multi-site inhibition of human plasma cholinesterase by cationic phenoxazine and phenothiazine dyes. Archives of Biochemistry and Biophysics 461(2), 294–298. [PubMed: 17428437]

Lehman CM, Frank EL, 2009 Laboratory Monitoring of Heparin Therapy: Partial Thromboplastin Time or Anti-Xa Assay? Laboratory Medicine 40(1), 47–51.

Luigi T, 1989 Randomised controlled trial of subcutaneous calcium-heparin in acute myocardial infarction. The SCATI (Studio sulla Calciparina nell'Angina e nella Trombosi Ventricolare nell'Infarto) Group. Lancet 2(8656), 182–186. [PubMed: 2568520]

Ma TY, Tang Y, Dai S, Qiao SZ, 2014 Proton-Functionalized Two-Dimensional Graphitic Carbon Nitride Nanosheet: An Excellent Metal-/Label-free Biosensing Platform. Small 10(12), 2382–2389. [PubMed: 24596304]

Martinez AW, Phillips ST, Whitesides GM, Carrilho E, 2010 Diagnostics for the Developing World: Microfluidic Paper-Based Analytical Devices. Anal. Chem. (Washington, DC, U. S.) 82(1), 3–10.

Maxwell LG, Goodwin SR, Mancuso TJ, Baum VC, Zuckerberg AL, Morgan PG, Motoyama EK, Davis PJ, Sullivan KJ, 2011 CHAPTER 36 - Systemic Disorders. Smith's Anesthesia for Infants and Children (Eighth Edition), pp. 1098–1182. Mosby, Philadelphia.

Mehta PK, Lee H, Lee K-H, 2017 Highly sensitive ratiometric detection of heparin and its oversulfated chondroitin sulfate contaminant by fluorescent peptidyl probe. Biosensors and Bioelectronics 91, 545–552. [PubMed: 28086125]

Muñoz EM, Linhardt RJ, 2004 Heparin-binding domains in vascular biology. Arteriosclerosis, thrombosis, and vascular biology 24(9), 1549–1557.

Murray DJ, Brosnahan WJ, Pennell B, Kapalanski D, Weiler JM, Olson J, 1997 Heparin detection by the activated coagulation time: A comparison of the sensitivity of coagulation tests and heparin assays. Journal of Cardiothoracic and Vascular Anesthesia 11(1), 24–28. [PubMed: 9058215]

Narins CR, Hillegass WB, Jr., Nelson CL, Tcheng JE, Harrington RA, Phillips HR, Stack RS, Califf RM, 1996 Relation between activated clotting time during angioplasty and abrupt closure. Circulation 93(4), 667–671. [PubMed: 8640994]

Ojito JW, Hannan RL, Burgos MM, Lim H, Huynh M, Velis E, Arocha M, Tirotta CF, Burke RP, 2012 Comparison of Point-of-Care Activated Clotting Time Systems Utilized in a Single Pediatric Institution. The Journal of Extra-corporeal Technology 44(1), 15–20. [PubMed: 22730859]

Perry DJ, Fitzmaurice DA, Kitchen S, Mackie IJ, Mallett S, 2010 Point-of-care testing in haemostasis. British Journal of Haematology 150(5), 501–514. [PubMed: 20618331]

Prisco D, Paniccia R, 2003 Point-of-Care Testing of Hemostasis in Cardiac Surgery. Thrombosis Journal 1, 1–1. [PubMed: 12904262]

Pu K-Y, Liu B, 2009 Conjugated polyelectrolytes as light-up macromolecular probes for heparin sensing. Adv. Funct. Mater 19(2), 277–284.

Pu K, Shuhendler AJ, Jokerst JV, Mei J, Gambhir SS, Bao Z, Rao J, 2014 Semiconducting polymer nanoparticles as photoacoustic molecular imaging probes in living mice. Nature Nanotechnology 9, 233.

Pu K, Zhen X, Zhang J, Huang J, Xie C, Miao Q, 2018 Macrotheranostic Probe with Disease-activated Near-infrared Fluorescence, Photoacoustic and Photothermal Signals for Imaging-guided Therapy. Angew Chem Int Ed Engl

Qin X, Chen H, Yang H, Wu H, Zhao X, Wang H, Chour T, Neofytou E, Ding D, Daldrup-Link H, Heilshorn Sarah C., Li K, Wu Joseph C, 2017 Photoacoustic Imaging of Embryonic Stem Cell-Derived Cardiomyocytes in Living Hearts with Ultrasensitive Semiconducting Polymer Nanoparticles. Advanced Functional Materials 28(1), 1704939. [PubMed: 30473658]

Shetty S, Ghosh K, Mohanty D, 2003 Comparison of four commercially available activated partial thromboplastin time reagents using a semi-automated coagulometer. Blood Coagulation Fibrinolysis 14(5), 493–497. [PubMed: 12851537]

Shi H, Sun H, Yang H, Liu S, Jenkins G, Feng W, Li F, Zhao Q, Liu B, Huang W, 2016 Polyfluorenes with Phosphorescent Iridium(III) Complexes for Time-Resolved Luminescent Biosensing and Fluorescence Lifetime Imaging [Erratum to document cited in CA159:314377]. Adv. Funct. Mater 26(36), 6505.

Shriver Z, Sasisekharan R, 2013 Heparin sensing Blue-chip binding. Nat. Chem 5(8), 644–646. [PubMed: 23881491]

Strohm Eric M., Berndl ESL, Kolios, Michael C, 2013 Probing Red Blood Cell Morphology Using High-Frequency Photoacoustics. Biophysical Journal 105(1), 59–67. [PubMed: 23823224]

Stylogiannis A, Prade L, Buehler A, Aguirre J, Sergiadis G, Ntziachristos V, 2018 Continuous wave laser diodes enable fast optoacoustic imaging. Photoacoustics 9, 31–38. [PubMed: 29387537]

Sun I-C, Emelianov S, 2018 Dual-imaging contrast agent for ultrasound and photoacoustic imaging: gas-generating plasmonic-core nanoconstruct (Conference Presentation). SPIE BiOS. SPIE

Takemoto CM, Streiff MB, Shermock KM, Kraus PS, Chen J, Jani J, Kickler T, 2013 Activated partial thromboplastin time and anti-Xa measurements in heparin monitoring: Biochemical basis for discordance. Am. J. Clin. Pathol 139(4), 450–456. [PubMed: 23525615]

Templeton DM, 1988 The basis and applicability of the dimethylmethylene blue binding assay for sulfated glycosaminoglycans. Connect. Tissue Res 17(1), 23–32. [PubMed: 3133157]

Tian J, Jarujamrus P, Li L, Li M, Shen W, 2012 Strategy To Enhance the Wettability of Bioacive Paper-Based Sensors. ACS Applied Materials & Interfaces 4(12), 6573–6578. [PubMed: 23151066]

Vera-Aguilera J, Yousef H, Beltran-Melgarejo D, Teng TH, Jan R, Mok M, Vera-Aguilera C, Moreno-Aguilera E, 2016 Clinical Scenarios for Discordant Anti-Xa. Advances in Hematology 2016, 4054806. [PubMed: 27293440]

Wahr JA, Shore AD, Harris LH, Rogers P, Panesar S, Matthew L, Pronovost PJ, Cleary K, Pham JC, 2014 Comparison of intensive care unit medication errors reported to the United States' MedMarx and the United Kingdom's National Reporting and Learning System: a cross-sectional study. Am J Med Qual 29(1), 61–69. [PubMed: 23656705]

Wang J, Chen F, Arconada-Alvarez SJ, Hartanto J, Yap L-P, Park R, Wang F, Vorobyova I, Dagliyan G, Conti PS, Jokerst JV, 2016 A Nanoscale Tool for Photoacoustic-Based Measurements of Clotting Time and Therapeutic Drug Monitoring of Heparin. Nano Lett 16(10), 6265–6271.

Wang J, Jeevarathinam AS, Humphries K, Jhunjhunwala A, Chen F, Hariri A, Miller BR, Jokerst JV, 2018 A Mechanistic Investigation of Methylene Blue and Heparin Interactions and Their Photoacoustic Enhancement. Bioconjugate Chemistry

Wong TTW, Zhang R, Zhang C, Hsu H-C, Maslov KI, Wang L, Shi J, Chen R, Shung KK, Zhou Q, Wang LV, 2017 Label-free automated three-dimensional imaging of whole organs by microtomy-assisted photoacoustic microscopy. Nature Communications 8(1), 1386.

Wright SJ, Murray WB, Hampton WA, Hargovan H, 1993 Calculating the protamine-heparin reversal ratio: a pilot study investigating a new method. J Cardiothorac Vasc Anesth 7(4), 416–421. [PubMed: 8400096]

Yoshimi Y, Yagisawa Y, Yamaguchi R, Seki M, 2018 Blood heparin sensor made from a paste electrode of graphite particles grafted with molecularly imprinted polymer. Sens. Actuators, B 259, 455–462.

You J-G, Liu Y-W, Lu C-Y, Tseng W-L, Yu C-J, 2017 Colorimetric assay of heparin in plasma based on the inhibition of oxidase-like activity of citrate-capped platinum nanoparticles. Biosensors and Bioelectronics 92, 442–448. [PubMed: 27836604]

Zemp RJ, Bitton R, Shung KK, Li M-L, Stoica G, Wang LV, 2007 Photoacoustic imaging of the microvasculature with a high-frequency ultrasound array transducer. Journal of biomedical optics 12(1), 010501. [PubMed: 17343475]

Zhang HF, Maslov K, Sivaramakrishnan M, Stoica G, Wang LV, 2007 Imaging of hemoglobin oxygen saturation variations in single vessels in vivo using photoacoustic microscopy. Appl. Phys. Lett 90(5), 053901/053901–053901/053903.

Zheng J, Ye T, Chen J, Xu L, Ji X, Yang C, He Z, 2017 Highly sensitive fluorescence detection of heparin based on aggregation-induced emission of a tetraphenylethene derivative. Biosensors and Bioelectronics 90, 245–250. [PubMed: 27914368]

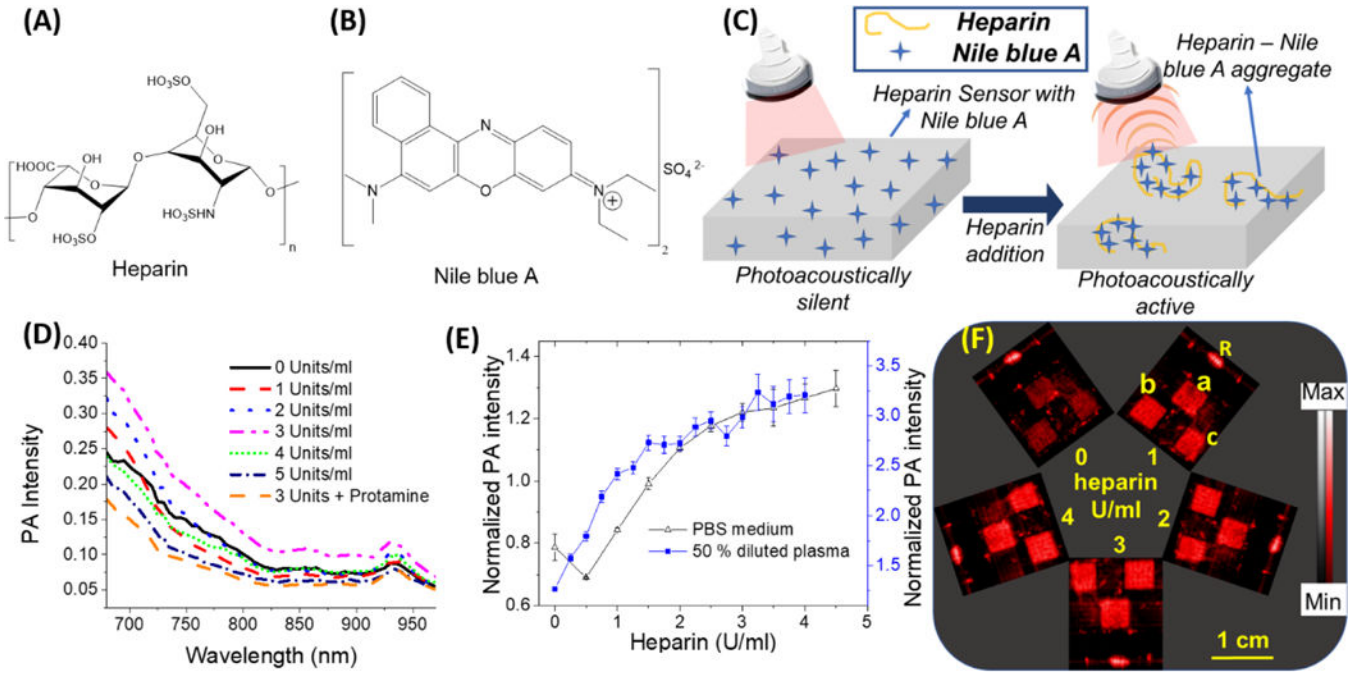

Fig. 1. Spectral and photoacoustic study of Nile blue A and cellulose based sensor in PBS and 50% diluted human plasma.

(A) Chemical structure of heparin. **(B)** Chemical structure of Nile blue A. **(C)** A schematic illustration of sensing mechanism of the sensors. Cationic dyes like Nile blue A form aggregates with heparin. The heparin-Nile blue A aggregates are much more photoacoustically active compared to non-aggregated Nile blue A molecules leading to an increased photoacoustic signal. **(D)** Photoacoustic spectrum of Nile blue A in aqueous solutions with different amounts of heparin. The maximum photoacoustic signal for Nile blue A was observed at 680 nm and hence 680 nm excitation was used throughout this study. **(E)** A plot of the ratio of average photoacoustic intensity of three sensors treated with increasing heparin concentrations normalized to the reference line (that does not change with heparin concentration) as a function of heparin concentration in PBS and 50% diluted plasma. **(F)** Photoacoustic image of three sensors (0.5 × 0.5 cm area) simultaneously treated with different heparin doses in 50% diluted pooled human plasma. The sensors labeled as a, b, and c are replicates with identical composition, and R is the reference line whose intensity remained constant regardless of heparin. The relative standard deviation for the diluted plasma assay is < 6.1%; the detection limit was 0.02 U/ml heparin in 50% diluted pooled human plasma. Error bars indicate the standard error of the three measurements.

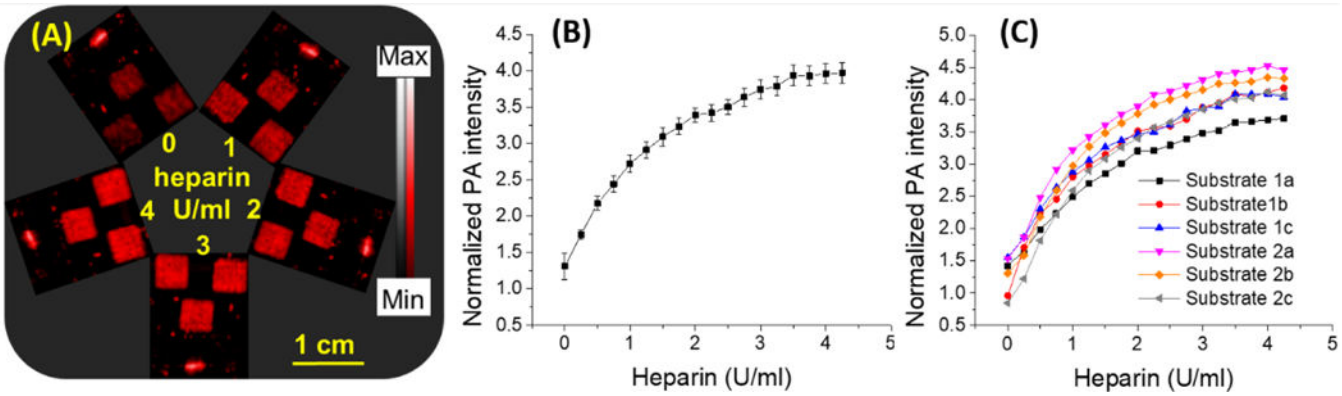

Fig. 2. Photoacoustic response of heparin sensor in undiluted human plasma.

(A) Photoacoustic image of three square-shaped sensors and reference graphite mark. The same set of sensors were subjected to different doses of heparin and imaged after each dose adjustment. **(B)** Plot of average normalized photoacoustic intensity of three sensors found in panel **(A)** versus heparin dose in human plasma. **(C)** Comparison of heparin response curves collected from two separate sets of experiments where 1a, 1b, and 1c represent results from independent experiment trial 1; 2a, 2b, and 2c are a second independent trial (a, b, and c are the different sensors; see Fig. S3). The results show that photoacoustic response of these sensor to heparin dose is very reproducible. Both the intraassay relative standard deviation and inter-assay relative standard deviation were <8.5%. The detection limit is 0.28 U/ml heparin in pooled human plasma. (0–2.0 U/ml). Error bars indicate the standard error corresponding to three measurements.

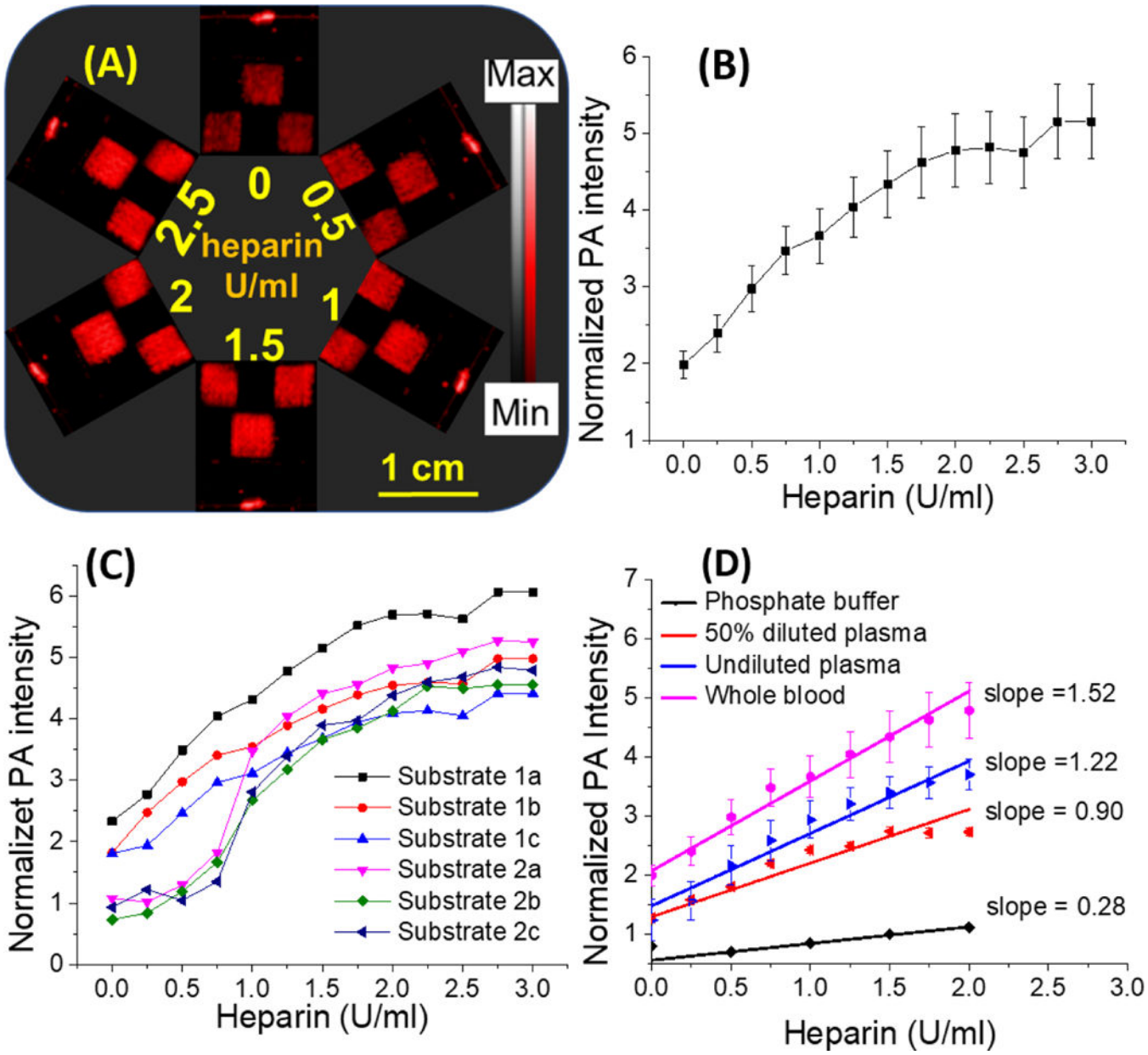

Fig. 3. Sensitivity of cellulose-based heparin sensor to different heparin doses in whole human blood.

The photoacoustic response of sensors was measured after immersing the sensor into whole human blood. Blood samples were collected from a single healthy donor and spiked with heparin. The sensors were dipped in this blood for one minute before being rinsed and imaged. **(A)** Representative photoacoustic images of the sensors (squares)— the photoacoustic response of the sensors increased with increasing amounts of heparin. The image represents the same set of sensors after sequential treatment with increasing amounts of heparin in whole blood. **(B)** Plot of normalized signal versus heparin in whole blood. The intra-assay reproducibility of these measurements is less than 17.5%. **(C)** Plot of normalized photoacoustic data for all sensors. This data shows the inter-assay reproducibility of

photoacoustic response in blood—differences were less than 17.4%. Panel **(D)** shows the photoacoustic response of sensors to different sample matrices. The slope (sensitivity) was highest in whole blood followed by plasma and PBS. Error bars indicate the standard error of the three measurements.

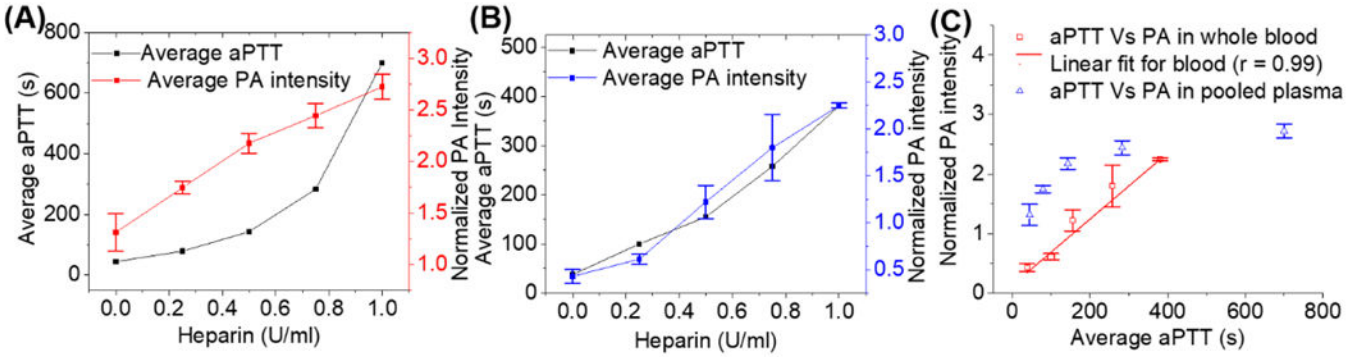

Fig. 4. Correlation of aPTT and photoacoustic response of cellulose-based heparin sensor in plasma and whole blood.

Panel **(A)** is the average normalized photoacoustic intensity of sensors from 0 to 1 U/ml heparin in plasma; the corresponding aPTT values were plotted against heparin concentrations in pooled plasma. The photoacoustic response was linear between 0 to 1.0 U/ml while aPTT values clearly deviated from linearity. Panel **(B)** shows the same experiment using whole human blood collected from a healthy donor. Panel (**C**) presents the linear correlation between the photoacoustic response of the sensor and aPTT values in pooled human plasma (Pearson's r = 0.86) and in whole human blood samples (Pearson's = 0.99).

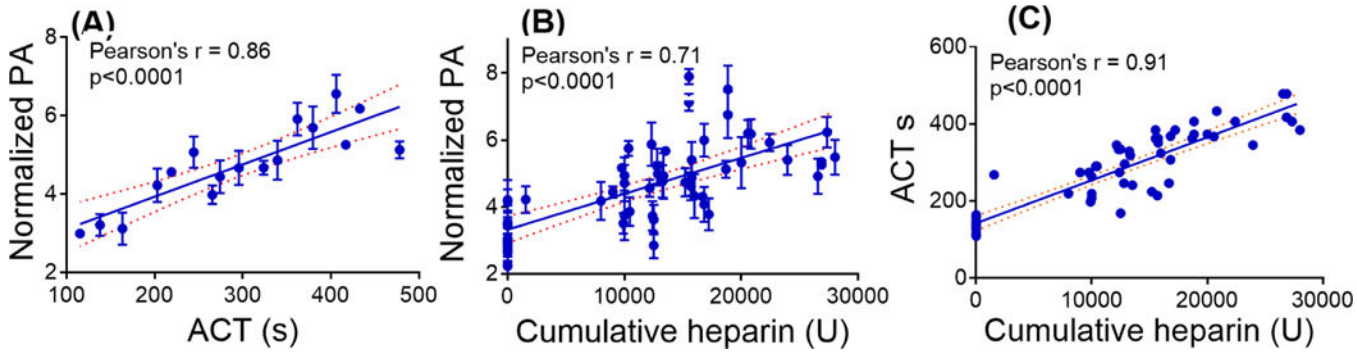

Figure 5. Photoacoustic response of sensors to clinical specimens collected from 16 patients undergoing cardiac procedures requiring heparin.

Panel **(A)** shows the photoacoustic response of sensors versus ACT. Here, the photoacoustic data were binned into 20-second ACT intervals from 109 to 478 s. Panel **(B)** presents the photoacoustic response as a function of cumulative heparin dose, and panel **(C)** shows linear correlation between ACT and cumulative heparin dose. The data corresponding to **(B)** and **(C)** were not binned. The correlation was linear for all three analyses (Pearson's $r > 0.7$). The dotted lines represent the 95% confidence interval (CI) band. The P value < 0.0001 indicates that the changes in photoacoustic intensity and ACT values are significantly correlated. Error bars in panels **(A)** and **(B)** indicate standard error.